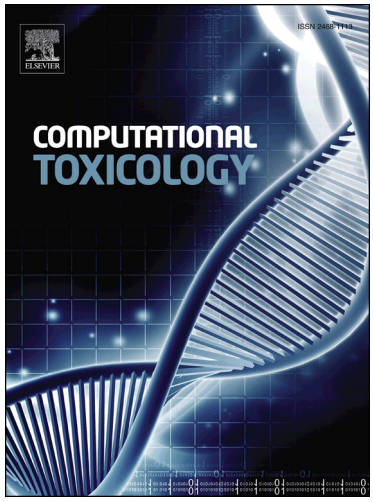

Quantitative AOP Based Teratogenicity Prediction for Mixtures of Azole Fungicides

Maria Battistoni, Francesca Di Renzo, Elena Menegola, Frederic Yves Bois

PII: S2468-1113(18)30142-7
DOI: https://doi.org/10.1016/j.comtox.2019.03.004
Reference: COMTOX 85

To appear in: *Computational Toxicology*

Received Date: 18 December 2018
Revised Date: 7 March 2019
Accepted Date: 13 March 2019

Please cite this article as: M. Battistoni, F. Di Renzo, E. Menegola, F.Y. Bois, Quantitative AOP Based Teratogenicity Prediction for Mixtures of Azole Fungicides, *Computational Toxicology* (2019), doi: https://doi.org/10.1016/j.comtox.2019.03.004

QUANTITATIVE AOP BASED TERATOGENICITY PREDICTION FOR MIXTURES OF AZOLE FUNGICIDES

Maria Battistoni*[1], Francesca Di Renzo [1], Elena Menegola[1], Frederic Yves Bois*[2].

[1]Department of Environmental Science and Policy, University of Milan, via Celoria 26, 20133 Milan, Italy.

[2]DRC/VIVA/METO, INERIS, Parc Technologique ALATA, 60550 Verneuil-en-Halatte, France.

* These authors contributed equally to this work

Corresponding author: Maria Battistoni

via Celoria, 26

20133 Milan, Italy

mail: maria.battistoni@unimi.it

Keywords (da 3 a 6)

Quantitative AOP, Azoles, Mixture, Craniofacial, Embryotoxicity

Abbreviations:

CI: Confidence interval

CYP26: Cytochrome P450 isoform 26

CYPRO: Cyproconazole

FLUCO: Fluconazole

FLUSI: Flusilazole

FON: Triadimefon

NCCs: Neural crest cells

qAOP: Quantitative adverse outcome pathway

RA: Retinoic acid

WEC: Whole embryo culture

Abstract

Exposure of embryos to mixtures of environmental chemicals can result in congenital malformations. Mixture experiments can provide an indication of the joint effects of substances, but it is practically infeasible to test all possible combinations. The development of mechanistic approaches and integrated

models able to predict the effects of mixtures from the concentrations of their individual components, are crucial to assess mixtures associated risks. Azole fungicides can induce craniofacial defects, both after *in utero* and *in vitro* exposure. Results obtained *in vitro* have shown a significant enhancement of teratogenic effects after co-exposure to azoles in comparison to the single exposures. In this project, we evaluated the hypothesis that those molecules concur to imbalance the retinoic acid pathway in specific responsive embryonic tissues. We developed a quantitative adverse outcome pathway for craniofacial malformations, able to simulate the formation of the physiological retinoic acid gradient in the rat embryo hindbrain and its perturbation after exposure to cyproconazole, flusilazole, triadimefon and to their binary mixtures. The underlying system biology model was calibrated using *in vitro* data and is reasonably predictive of mixtures' effects for those azoles, thereby confirming the plausibility of the hypothesized pathogenic pathway. This quantitative AOP could have mechanistic or predictive applications in pesticides risk assessment.

1. Introduction

In the last years, the effects on human health and environment resulting from the exposure to multiple chemicals have become an item of concern. Humans and all other organisms are typically exposed to mixtures of chemicals, present in water, air, soil, food or consumer products (Feron et al. 1998; Groten 2000). Exposure of animal embryos to some pesticides can result in developmental defects including a range of craniofacial deformities like cleft lip or cleft palate, which are one of the most frequent in humans (1:700 live births) (Mossey et al. 2009). To enable predictive assessments of those health effects by mixtures of chemicals, it is essential to develop approaches, such as quantitative adverse outcome pathways (qAOPs), able to predict mixtures' effects from concentrations of their individual components (Feron and Groten 2002; Cheng and Bois 2011; Bois et al. 2017). In addition, the integration of evidence from alternative *in silico* or *in vitro* methods in qAOPs contributes to the reduction of toxicity testing in animals (a potentially endless task when it comes to mixtures). The eventual complete replacement of animal experiments is also important for ethical, scientific and economic reasons.

Retinoic acid (RA), the active metabolite of vitamin A, is a well-known morphogen in invertebrates and vertebrate embryos and it is considered the main molecule involved in craniofacial morphogenesis (Suzuki et al. 1999). Both deficiency and excess of embryonic RA are related to malformations at multiple portions, including craniofacial defects in humans and animals (Warkany and Schraffenberger 1944; Lammer et al. 1985; Hathcock et al. 1990; Morriss-Kay 1992; Browne et al. 2014; Piersma et al. 2017). In presence of excess of RA, postimplantation rodent whole embryo cultures (WEC) show specific defects, including branchial arch (the embryonic facial primordia) abnormalities (Klug et al. 1989; Menegola et al. 2004). The postimplantation rodent whole embryo culture (WEC) is an *in vitro* technique validated by the European Centre for the Validation of Alternative Methods (ECVAM) in 2001 (Anon 2002) as a screening and/or prioritization tool for pharmaceutical, agricultural, and industrial chemicals.

There are several possible causes of imbalance in RA concentrations and many substances are able to alter craniofacial development: valproic acid, thalidomide, retinoids, ethanol and some drugs and pesticides such as the class of the azoles fungicides (Morriss and Steele 1974, 1977; Steele et al. 1987; Klug et al. 1989; Kotch et al. 1995; Hansen et al. 1999; Parman et al. 1999; Menegola et al. 2013). Azoles are synthetic antifungal compounds, derived from triazole or imidazole, sold annually in thousands of tons for the purpose of plant protection (Hof 2001). Their large use in agriculture and presence as residues in food carry the potential for human exposure. In addition to environmental exposure, humans can be exposed to some azole fungicides for the treatment of local or deep fungal infections (Zarn et al. 2002; EFSA 2009). The specific teratogenic effect of some azole fungicides has been investigated using postimplantation rat WEC. Embryos exposed to single azoles develop abnormal branchial structures, similar to those induced by excess of RA, related to the abnormal hindbrain segmentation and abnormal neural crest cells (NCCs) migration and compaction (Menegola et al. 2000, 2001, 2003, 2005a, 2005b, 2006a, 2006b; Di Renzo et al. 2007, 2011a, 2011b). The postulated mechanism of action was the inhibition of CYP26 enzymes (involved in RA degradation during early embryonic development), with the consequent increase in RA local content (Menegola et al. 2006a, 2006b; Marotta and Tiboni 2010). The observation in rodent embryos that the co-exposure to sub-teratogenic doses of both RA (0.025 µM) and fluconazole (FLUCO) (62.5 µM) leads to the same phenotype as the teratogenic doses of RA and FLUCO alone, definitively supported the hypothesis of local increase of RA as key event in azole teratogenicity (Menegola et al. 2004, 2006a).

In addition, data previously obtained by Menegola *et al.* (2013) described an increase of the teratogenic effects (reduction and fusion of branchial arches) in postimplantation rat WEC in presence of mixtures of azole fungicides, including triadimefon (FON), flusilazole (FLUSI) and cyproconazole (CYPRO), compared to the single exposures. Since in standard human risk assessment, chemicals thought to exhibit their effects through common mechanisms are assumed to show dose-additivity and are grouped together (cumulative risk assessment) (Moretto 2008), is it likely that mixtures of azole fungicides could show dose-additivity too.

The aim of this work was therefore to develop a quantitative AOP able to integrate *in silico*, *in vitro*, *in vivo* evidence, and to simulate the formation and perturbation of physiological RA levels in the rat embryo hindbrain. A successful prediction of RA perturbation in embryos after exposure to binary mixtures azole, based on the hypothesized mechanism, would both test and strengthen our mechanistic hypothesis.

2. Materials and Methods

2.1 In vitro experiments

2.1.1 Material and selection of compound concentrations

Experimental data on frequencies of malformations of the branchial arches following exposure to RA, individual azoles (CYPRO, FLUSI, FON) and binary mixtures (increasing concentrations of one azole + the lowest-effect concentration of another azole), obtained in our laboratory in Milano (Di Renzo et al. 2019), were used in this study (Table 1). All the tested compounds were purchased from Sigma, Italy. The medium used for the extraction of embryos from the uteri was sterilised Tyrode solution (Sigma); the medium used for the post-implantation whole embryo culture was undiluted heat inactivated rat serum added with antibiotics (penicillin100IU/mL culture medium and streptomycin 100µg/mL culture medium, Sigma). The concentrations of test molecules were selected from previous published experiments on rat WEC to gradually achieve the maximum degree of severity for branchial malformations: RA 0.025–0.5µM, FLUSI 1.56–9.375 µM, FON 6.25–250 µM, and CYPRO 7.8–250 µM. For each dose-response experiment, a group was exposed to the relative solvent (dose 0).

2.1.2 Embryo culture

Virgin female CD:Crl rats (Charles River, Calco, Italy), housed in a thermostatically maintained room (T=22± 2°C; relative humidity 55 ± 5%) with a 12-h light-dark cycle (light from 6:00 a.m. to 6:00 p.m.), and free access to food (Italiana Mangimi, Settimo Milanese, Italy) and tap water, were caged overnight with males of proven fertility. All animal use protocols were approved by the Ministry of Health, Department for Veterinary Public Health, Nutrition and Food Safety committee. The animals were treated humanely and with regard for the alleviation of suffering. Embryos were explanted from untreated pregnant rats at E9.5 (early neurula stage, 1–3 somites; day of positive vaginal smear = 0) and cultured according to the New method (1978) in 20-mL glass bottles (five embryos/bottle), containing 5mL of culture medium. The culture was performed at least in triplicate for each group. The bottles, inserted in a thermostatic (37.8°C) roller (30rpm) apparatus, were periodically gas equilibrated according to Giavini et al. (1992). After 48 h of culturing, the embryos were morphologically examined under a dissecting microscope to evaluate any branchial or morphological abnormality. A morphological score was determined according to Brown and Fabro (1981). Overall, no branchial arch malformations were observed in 201 control embryos.

2.2 qAOP model

AOPs describe a causal sequence of events, starting from one or more molecular initiating events, followed by a sequence of measurable key events, leading to an adverse outcome (Villeneuve et al. 2014). They help organize information from a wide range of sources (*in silico*, *in vitro*, *in vivo*, etc.) for use it in weight of evidence schemes when assessing the plausibility of a link between a chemical's effects on individual events and adverse outcomes of interest (Madden et al. 2014). However, for prediction of risk from exposure to single chemicals or mixtures, quantitative AOPs (qAOPs) that provide dose-response and time-course predictions (Leist et al. 2017, Zgheib et al. submitted) are likely to be more valuable than qualitative AOPs. We therefore developed a biologically-based quantitative model for predicting the impact of retinoic acid morphogenic gradient disruption by CYP26 inhibitors on craniofacial skeletal malformation that aligns with a corresponding AOP. It has been suggested that azole fungicides act via this pathway (Menegola et al. 2006a; Marotta and Tiboni 2010).

2.3.1 RA gradients formation, function and disruption in organogenesis

According to the literature, the synthesis of RA is catalysed by ADH7 and it is degraded by cytochrome P450 isoforms CYP26A1, CYP26B1, and CYP26C1 (Morriss-Kay 1992). The generation and diffusion of RA has been proposed to form a gradient that patterns the hindbrain into seven rhombomeres (r1-7) from which the neural crest cells (NCCs) migrate and colonize the future cranio-facial structures (White et al. 2007; Schilling et al. 2012). Because morphogens act at a distance from their source of production, eliciting distinct cellular responses in a concentration-dependent manner (Rogers and Schier 2011), their action needs to be robust and precise. RA, in fact, induces the synthesis of CYP26A1, which in turn specifically degrades it (White et al. 2007), inducing a negative feedback loop regulating RA levels. In addition, the level of CYP26a1 mRNA in the hindbrain is up-regulated by RA and fibroblast growth factor (FGF) (Reijntjes et al. 2005). This self-enhanced degradation of RA is a mechanism that enhances RA gradient robustness. Despite that control, severe malformations of the face can result either from a generalized RA imbalance or from an ectopic localization of RA in rhombomeres, with a subsequent ectopic expression of growth factors and genes in the hindbrain and rhomboencephalic NCC-derived tissues (Morriss-Kay 1992; Osumi-Yamashita et al. 1994; Mark et al. 1995; Whiting 1997; Schneider et al. 2001).

The CYP26 enzymes therefore play a central role in protecting the developing embryo from supra-physiological levels of RA. In particular, the crucial role of CYP26A1 during development is underlined by the notion that *Cyp26a1*-/- mutant embryos show abnormal hindbrain specification, abnormal neural crest cell migration and abnormal anterior branchial arches (Sakai 2001; Abu-Abed et al. 2002; Uehara et al. 2007). Previous studies indicates that *Cyp26a1* is initially expressed in the anterior neural plate during gastrulation (Kudoh et al. 2002) and that it first establishes the anterior boundary of the RA signal at r2–r3 (Sirbu 2005). CYP26A1 is also required for exogenous RA treatments to rescue RA-deficient embryos (Hernandez et al. 2007). Thus, CYP26A1 seems to have a key role in the hindbrain, distinct from that of the other two isoforms CYP26B1 or CYP26C1 (which are not induced in the nervous system by RA) as the major RA-degrading enzyme (White et al. 2007). Considering the essential role of CYP26A1 during the initial phases of the embryonic development, only CYP26A1 was considered in the present model. CYP26A1 inhibition is therefore a likely molecular initiating event for RA gradient disruption.

Furthermore, exposure to FLUCO has been linked to an increased expression of CYP26A1 mRNA (Tiboni et al. 2009).

The structure of the qAOP we propose for skeletal craniofacial defects therefore includes (Figure 1): (1) CYP26 inhibition, (2) imbalance of RA gradients in the hindbrain, (3) altered RA-regulated gene expression, (4) altered hindbrain NCC migration and compaction, (5) embryonic branchial arch defects, (6) craniofacial skeletal defects (the adverse outcome).

2.3.2 qAOP development strategy

Besides mechanistic information, the data we have are direct observations of branchial arch malformations after exposure of embryos to RA or azoles. We therefore first established a dose-response relationship between RA and the probability of occurrence of malformations. For this, we used a multistage dose-response model. Given this relationship, to link exposures to azoles to observed malformations we developed a systems biology model describing RA gradient formation in the hindbrain and its potential disruption by the three azoles tested. The data on the effect of individual azoles allowed us to obtain estimates of their CYP26A1 inhibition constants, through Bayesian calibration. After that calibration step, the model was used purely predictively to simulate the effect of exposures to mixtures of the azoles. The predictions were then simply compared to the observed mixtures' effects.

2.3.3 RA kinetics equations

The first part of our model describes the formation of RA gradient during the early development of a rat embryo hindbrain and its perturbation after exposure to CYP26A1 inhibitors (here, FLUSI, FON, and CYPRO). We focus on development between days 9.5 and 10 post-fertilization, which is the sensitive window for azole fungicides exposures (Di Renzo et al. 2011b).

The system biology model equations are adapted from Goldbeter et al. (2007). Those authors focused on mesenchymal presomitic mesoderm, rather than on the hindbrain, where the control details are slightly different. Therefore we did not include FGF inhibition by RA, and we considered parallel linear gradients in the rate of synthesis of RA and in the amount of FGF (White et al. 2007; Schilling et al. 2012). The model state variables are the concentrations of RA (*RA*), *cyp26a1* mRNA (*mRNA*), CYP26A1 protein (in

active form) (*CYP26*) and FGF protein (*FGF*). The time evolution of these variables at a distance *x*, in units of average cell length, from the beginning of the 7th rhombomere (up to the end of the 1st rhombomere, *i.e.*, covering the hindbrain), is governed by the following set of differential equations.

RA synthesis is catalysed along a linear gradient in distance *x* by aldehyde dehydrogenase (ADH), it is also metabolized by CYP261A and other enzymes:

$$\frac{\partial RA(x,t)}{\partial t} = k_{syn,RA} \cdot ADH \frac{L-x}{L} - k_{met,RA} \cdot CYP26(x,t) \cdot RA(x,t) - k_{deg,RA} \cdot RA(x,t) \quad (1)$$

where parameters $k_{syn,RA}$ and $k_{met,RA}$ measure respectively the rate of synthesis of RA by ADH and the first order degradation rate of RA by CYP26A1, and $k_{deg,RA}$ represents the rate of nonspecific degradation of RA. L is the number of the hindbrain cells ($L = 50$) at the considered stage.

CYP26 mRNA synthesis is increased by RA and decreased by FGF, with a first order degradation rate:

$$\frac{\partial mRNA(x,t)}{\partial t} = k_{trs} + v_{max} \cdot \frac{RA(x,t)^2}{k_{act}^2 + RA(x,t)^2} \cdot \frac{k_{inh}^2}{k_{inh}^2 + FGF(x,t)^2} - k_{deg,mRNA} \cdot mRNA(x,t) \quad (2)$$

where k_{trs} is a baseline transcription rate, v_{max} is the maximum increase in transcription rate by the concurrent actions of RA of FGF (described by Hill functions with cooperativity degree 2), k_{act} is the activation constant by RA, k_{inh} the inhibition constant by FGF, and $k_{deg,mRNA}$ a first order degradation rate constant.

CYP26A1 is synthesized with translation rate constant k_{trd}, degraded with first order rate constant k_{deg}, and inactivated by FLUSI, FON and CYPRO (which are constant parameters set at the nominal exposure value for each chemical) with inhibition rate constants k_{inh_FLUSI}, k_{inh_FON}, and k_{inh_CYPRO}, respectively:

$$\frac{\partial CYP26(x,t)}{\partial t} = k_{tsl} \cdot mRNA(x,t) - (k_{deg,CYP} + k_{inh,FLUSI} \cdot FLUSI + k_{inh,FON} \cdot FON + k_{inh,CYPRO} \cdot CYPRO) \cdot CYP26(x,t) \quad (3)$$

FGF is synthesized at a rate proportional to $k_{syn,FGF}$, higher in the posterior hindbrain than in the anterior hindbrain, and degraded with first order rate constant k_{deg}.

$$\frac{\partial FGF(x,t)}{\partial t} = k_{syn,FGF} \cdot \left(1 - \frac{x}{L}\right) - k_{deg,FGF} \cdot FGF(x,t) \quad (4)$$

To simulate the concentration of RA, CYP261A mRNA, CYP26A1 and FGF, at different times and different locations in the hindbrain, the equations were solved by numerical integration. We ran the simulations until stable gradients were established. About an hour of simulated time was needed to obtain stable gradients when starting from the initial concentration values (all at 0.1 nM) used in Goldbeter *et al.* (2007).

Most model parameter values were set to those reported in Goldbeter et al. (2007), or to other published values when those were more relevant (see Table 2). The CYP26 mRNA transcription activation by RA constant (k_{act}) and the transcription inhibition by FGF constant (k_{inh}) were adjusted so that the RA baseline concentration matched the value given in Duester (2008) and the shape of the RA and CYP26 gradients matched the description given by Schilling et al. (2012). The CYP26 inhibition constants by azoles were numerically estimated via Bayesian calibration (Bois 2009a). Parameter values are reported in Table 2.

2.3.4 Malformation risk model

To predict the probability of malformation as a function of (excess) RA concentrations in the hindbrain we used a multistage model. The effective dose was taken to be RA concentration increase over baseline (RA_{base}), at the middle of the hindbrain (distance x equal to 25) in steady-state conditions (at time t_{ss}, in our case at 48 hours). The RA baseline concentration was set to 26 nM (Duester 2008).

$$D = RA(25, t_{ss}) - RA_{base} \tag{5}$$

$$P = 1 - exp(-Q_0 - Q_1 \cdot D) \tag{6}$$

The Q_0 and Q_1 parameters were estimated via Bayesian calibration (see the Statistical methods section).

2.3.5 Statistical methods

Five parameters of the malformation qAOP (Q_0, Q_1, k_{inh_FLUSI}, k_{inh_FON}, and k_{inh_CYPRO}) were calibrated so that the prediction of probability of craniofacial malformations matched the frequency data obtained after exposure of embryos to single chemicals (RA, FLUSI, FON, or CYPRO). In each case, we used Bayesian calibration (Bois 2009a). The measured counts of branchial arch malformation following 48 h of exposures to RA or to the single azoles (Table 1) were assumed to be binomially distributed with a probability P given

by the multistage model (Eq. 6). The priors were set to uninformative uniform distributions. Given the prior and the data, Markov-chain Monte Carlo (MCMC) simulations were performed. In each case, two MCMC chains were run in parallel for 10,000 iterations. The last 5000 samples from each chain were kept for inference and predictive simulations. Convergence of the chains was assessed using Gelman and Rubin R_{hat} criterion. Convergence was achieved in all cases.

2.3.6 Software

All model simulations and MCMC calibrations were performed with *GNU MCSim* version 6.0.1 (www.gnu.org/software/mcsim) (Bois and Maszle 1997; Bois 2009a). All plots and miscellaneous calculations were created with *R*, version 3.4.4 (cran.r-project.org) (R Development Core Team 2013).

3 Results

3.1 Effects of exposure to RA, azoles and their binary mixtures on embryo development

As reported in Di Renzo et al. (2019), dose-related teratogenic effects were detected in embryos exposed to the different chemicals. The specific target for all tested azoles was the branchial apparatus, which was also affected by RA exposure. In the control group no abnormalities has been observed. All the tested RA and CYPRO concentrations resulted effective for branchial arch abnormalities, while the branchial apparatus was affected only after exposure to FON at concentrations of 7.8 µM or greater and FLUSI at concentrations of 3.125 µM or greater. The co-exposure to the increasing concentrations of one azole and the lowest-effect concentration of another azole enhanced the incidence of branchial arch malformations. In mixture with FON, the no-effect tested concentration of FLUSI (1.526 µM) was teratogenic and the lowest effect concentration of CYPRO (7.8 µM) enhanced its teratogenic effectiveness to the 80%. Finally, in mixture with FLUSI, the no-effect tested concentration of FON (6.25 µM) produced a severe teratogenic effect with the 100% of malformed embryos (Table 1).

3.2 RA gradient profiles in the rat embryo hindbrain

We obtained the baseline gradients after adjusting the CYP26 mRNA transcription activation by RA constant (k_{act}) and the transcription inhibition by FGF constant (k_{inh}), as well as its perturbation during constant exposures to various levels of FLUSI (Figure 2). The inhibition constant for FLUSI was set to the mode value given in Table 3. The value of the baseline gradient is 26 nM in the middle of the hindbrain, as indicated in Duester (2008). The shape of the gradients matched the description given by Schilling et al. (2012), with an accumulation of CYP in the anterior region, and higher concentrations of RA and FGF in the posterior region. Exposures to a CYP26A1 inhibitor have a profound effect on RA concentrations. Note that, as observed by Tiboni et al. (2009) for FLUCO, exposure to a CYP26A1 inhibitor leads to an increased expression of CYP26A1 mRNA.

3.3 qAOP calibration

The fit of the multistage model to experimental data on the percentage of branchial arch malformations caused by increasing RA concentrations (Figure 3) is quite good given the uncertainty in the data (the dark grey area marks the 95% confidence region of the malformation probability estimates, the light grey area the 95% confidence regions of model predictions for groups of 12 embryos, *i.e.*, for data predictions). The limited sample size of the data leads to increased uncertainty and to discrete confidence bounds (hence the staircase aspect of the data confidence intervals). In that case, RA exposures are exogenous and already represent increases over background. Therefore, for the calibration of the multistage model parameters, the value of RA_{base} was set to zero. A summary of the posterior distributions of the parameters Q_0 and Q_1 is given in Table 3. Note that the mode (best) value of Q_0 is very close to zero.

The data of the fitted relationships between FLUSI, FON, or CYPRO concentrations and branchial arch malformations are well reproduced (Figure 4). To obtain those fits, the parameters Q_0 and Q_1 of the multistage link between RA excess concentration in the hindbrain and malformations were set to their mode (see Table 3). The value of RA_{base} was set to 26 nM, because RA exposure is endogenous here and RA baseline value needs to be subtracted. The inhibition constants for the three azoles were calibrated with MCMC simulations to obtain a sample from their posterior distributions, which are summarized in Table 3. The uncertainty resulting from the unavoidable measurement errors and modelling approximations is

reflected by the grey areas, which correspond to the 95% confidence interval for the probability prediction curves (dark grey) and for the data themselves (light grey).

All parameters values being determined, the qAOP was then used for predictions. The predicted relationship between concentrations of the three azoles studied and the internal concentration of RA in the mid-hindbrain showed that the increase in RA concentrations is linear with exposure in each case (Figure 5). This is the net effect of CYP26A1 inhibition, subsequent decrease in RA metabolism, feedback to increased CYP26A1 mRNA transcription and CYP26A1 synthesis increase. Note that the feedback loop has in this case a simple linear dampening effect.

3.4 Prediction of azoles' mixtures effects

Then, pure model predictions of the percentage of branchial arch malformations for binary mixtures of FLUSI at different concentrations mixed with 12.5 µM FON, different concentrations of FON mixed with 3.125 µM FLUSI, and different concentrations of CYPRO with 7.8 µM FON was obtained (Figure 6). For comparison with the predictions, experimental data are superimposed but they were not used in the calibration process and just serve as a validation of the predictions. The mixture effects are quite strong, and the malformation data are slightly underestimated by model predictions, but they fall within the 95% confidence intervals of the model predictions. Note that the "zero" dose data points in Figure 6 do not correspond to the absolute control of Table 1, but to the data point of the co-exposure azole at the concentration used (from its single exposure data).

4 Discussion

We developed a qAOP for the occurrence of cranio-facial malformations in rat embryos following inhibition of RA metabolism by CYP26A1. RA is a very important morphogen, considered to be the main molecule involved in cranio-facial morphogenesis (Suzuki et al. 1999). It is known from literature that just a little imbalance in RA concentrations could alter the cranio-facial development with also severe consequences (Morriss-Kay 1992; Osumi-Yamashita et al. 1994; Mark et al. 1995; Whiting 1997; Schneider et al. 2001). The underlying model parameters were calibrated in a Bayesian framework on the

basis *in vitro* data on the developmental effects of three azoles alone. The qAOP was then used to predict internal RA levels in hindbrain and mixture effects following co-exposure to those azoles. Data and model predictions agree well, and our results are coherent with our hypotheses about the structure of this pathogenic pathway.

We benefited from a homogeneous dataset with well-designed experiments. The potential inhibition of RA synthesis by ethanol (17 mM), used as solvent of the azoles, was also evaluated. Since it made no difference in the results (data not shown), we chose to not include an effect of ethanol in the model.

The model is not perfect though, and the predicted effects somewhat underestimated the experimental results. This may be due to the fact that we only considered action of the azoles on the CYP26A1 isoform while at least three isoforms are expressed or partially co-expressed in early embryonic tissues (including branchial arches) (White and Schilling 2008). CYP26A1 is initially expressed in the anterior neural plate during gastrulation (Kudoh et al. 2002) and forms a boundary at presumptive r2/r3 (Pennimpede et al. 2010). This is followed by the later expression of CYP26A1 in r2 and Cyp26C1 in r2 and r4 (Fujii 1997; Abu-Abed et al. 2002; Tahayato et al. 2003; Uehara et al. 2007). From studies with *Cyp26a1*-/- mutant embryos, showing abnormal hindbrain specification, abnormal neural crest cell migration and abnormal anterior branchial arches (Sakai 2001; Abu-Abed et al. 2002; Uehara et al. 2007), Cyp26A1 seems to have a key role in the developing hindbrain to precisely restrict the field of endogenous RA signalling (White and Schilling 2008). In contrast to Cyp26A1, Cyp26B1 expression appears later and in a more dynamic pattern in the hindbrain in mice initially in r3 and r5 and later in r2–6 (MacLean et al. 2001). These patterns suggest that Cyp26B1 creates a new sink for RA within the central hindbrain (r3–5) at the end of gastrulation that eventually covers all but the most posterior rhombomeres. Cyp26C1 expression initially appears in the head mesenchyme at E7.5 (Uehara et al. 2007), and is then expressed after gastrulation in r4 earlier than that of Cyp26B1 in r3 and r5 (MacLean et al. 2001; Sirbu 2005). These patterns suggest that Cyp26C1, like Cyp26B1, forms a sink for RA within the central rhombomeres (r2– 6) of the hindbrain that both reduces RA within cells that express it and helps shape gradients of RA in adjacent cells.

It is known from literature, in fact, that morphogenetic gradients during hindbrain development are more complex than a simple concentration gradient of endogenous RA. Sirbu (2005) demonstrated the existence of dynamic shifting boundaries of hindbrain RA activity. His study showed that a stable RA gradient is not

established across the hindbrain, but the initial gradient of RA entering the posterior hindbrain is converted by CYP26s isoforms into RA boundaries that shift over time such that anterior tissues receive a short pulse of RA and posterior tissues receives a long pulse of RA. In particular, RA generated by RALDH2 in paraxial mesoderm initially travels as far anteriorly as presumptive r3 forming an early RA signalling boundary at r2/r3 just posterior to the RA-degrading enzyme Cyp26A1 expression domain. However, this boundary shifts posteriorly to the r4/r5 border to the expression of Cyp26C1 in r4. Hence, the hindbrain utilizes the RA-degrading function of Cyp26s isoforms to establish shifting boundaries of RA activity. Sirbu (2005) also showed that the initial RA boundary at r2/r3 is independent of RA activity, as Cyp26A1 expression does not require RA, but that the shift to an r4/r5 boundary is dependent upon RA to activate Cyp26C1 expression in r4. This pattern is essential for the specification of both rhombomeres and rhombomeric neural crest cells (NCC) migrating to the corresponding branchial region (Trainor and Krumlauf 2000). These results provide strong evidence that the combined action of all three Cyp26s, differentially expressed in embryonic tissues, are required to pattern the A-P axis of the hindbrain (Figure 7).

The possibility of a different affinity of different azoles for the expressed CYP26 isoforms could explain the underestimation of the predicted effects when compared to experimental results and it should be taken in account for a future version of the model. Moreover, inhibition by azoles of other cytochromes expressed in embryos at early stages such as CYP51, CYP2S1, and CYP11A1, all involved during the synthesis of cholesterol, steroids, and other lipids (Choudhary et al. 2003) could also be considered. We included a general term covering RA degradation by other enzymes than CYP26A1 in the RA kinetic equation, but that simple term cannot account for the subtle time-evolving controls mentioned above. Note also that, in the absence of data on endogenous RA levels in the hindbrain, we had to make the assumption that external exposure to RA resulted in the same increase in malformations as internal increase in RA levels. This is clearly an approximation, as we have no proof that hindbrain RA levels increase proportionally to external exposures. To develop and validate a more sophisticated model, we would need data on RA and other morphogens concentration in the hindbrain as a function of time and xenobiotic exposure concentrations.

In the simple model we developed, the various azoles act with the same mode of action, and the way in which they enter Eq. 3 amounts to dose additivity. In fact, the terms involving FLUSI, FON, and CYPRO in Eq. 3 could be grouped with their relative potencies normalised to that of FLUSI for example, as in:

$$k_{inh,FLUSI}\left(FLUSI + \frac{k_{inh,FON}}{k_{inh,FLUSI}}FON + \frac{k_{inh,CYPRO}}{k_{inh,FLUSI}}CYPRO\right)$$

More chemicals acting by the same mechanism could easily be included with this approach. On the other hand, our results partly support the use of dose addition for malformations induced by azoles, even when using simpler dose-response models.

While the results presented show that our qAOP can simulate and predict malformation risk due to single azoles or their mixtures, we stayed within the framework of the WEC assay and did not attempt to extrapolate them to humans. This would require at least some pharmacokinetic modelling and the verification that hindbrain development mechanisms are sufficiently similar in humans and rats to warrant the extrapolation. That relates more to the assumed ability of the WEC to assess hazard and risks to human than to the accuracy of our AOP model. Anyway, CYP26 is one of the cytochrome P450 specifically expressed in vertebrate embryos during development, with more than 61% identity identified in aminoacidic sequence in fish, chicken and mammals. Such conservation in the sequence supports a high conservation of functions (Stoilov et al. 2001; Abu-Abed et al. 2002). Similar to mammalian embryos, other vertebrate (the frog *Xenopus laevis*), and invertebrate (the ascidian *Phallusia mammillata* and *Ciona intestinalis*) embryos showed congenital malformations similar to those obtained in mammals after azole embryo exposure. (Groppelli et al., 2005; Pennati et al., 2006; Zega et al., 2009).

5 Conclusion

The large use of many substances able to alter craniofacial development in agriculture (Gordon and Shy 1981) and their presence as residues in food, carry the potential for human exposure to their mixtures. Despite the limitations discussed above, our model has potential mechanistic and predictive applications for risk assessment of exposures to mixtures of azoles, or substances acting with the same mode of action on the RA pathway. Ideally, the underlying AOP and its quantitative counterpart should be further developed with data on missing key-events (internal RA and other morphogens' concentrations, omic markers of NCC migration initiation and control, etc.) and an AOP description will be add to the AOP-Wiki (http://aopwiki.org). The AOP-Wiki was developed as a user-friendly, open-source interface that

facilitates both sharing of AOP knowledge and collaborative AOP development (Villeneuve et al. 2014). Indeed, AOPs will provide a relevant construct to organize and share data and information, to promote collaboration between experts in various areas and research and the regulatory risk assessment community and to support more predictive approaches to regulatory toxicology (OECD 2018). The collection and the assembly of the supporting evidence for each key-event description will contribute to the completion of our AOP proposal, which has been submitted to the OECD AOP development Programme.

To arrive at realistic assessments of human health effects from exposure to mixtures, the development of approaches able to predict mixtures' effects from concentrations of their individual components is essential (Bois et al. 2017; Bois 2009b; Cheng and Bois 2011). In this context, the AOP/qAOP framework is useful for integrating *in vitro* test results, *in silico* estimates, *in vivo* data, and computational systems biology. We hope that our research will provide a better understanding of the toxicity mechanisms of single and combined chemicals affecting the skeletal craniofacial pathway, and better *ab initio* predictions of developmental toxicity.

6 Acknowledgements

The research leading to these results received funding from the European Union's Horizon 2020 research and innovation program under grant agreement 633172 (Euromix).

7 Conflict of interest

The authors declare that they have no conflict of interest.

8 References

Abu-Abed S, MacLean G, Fraulob V, Chambon P, Petkovich M, Dollé P. 2002. Differential expression of the retinoic acid-metabolizing enzymes CYP26A1 and CYP26B1 during murine organogenesis. Mech Dev 110:173–177; doi:10.1016/S0925-4773(01)00572-X.

Anon. 2002. INVITTOX protocol no. 68. Embryotoxicity testing using a whole embryo culture WEC procedure, List of INVITTOX protocols.

Bois FY. 2009a. GNU MCSim: Bayesian statistical inference for SBML-coded systems biology models. Bioinformatics 25:1453–1454; doi:10.1093/bioinformatics/btp162.

Bois FY. 2009b. Physiologically-based modelling and prediction of drug interactions. Basic Clin Pharmacol Toxicol 106:154–161; doi:10.1111/j.1742-7843.2009.00488.x.

Bois FY, Golbamaki-Bakhtyari N, Kovarich S, Tebby C, Gabb HA, Lemazurier E. 2017. High-throughput analysis of ovarian cycle disruption by mixtures of aromatase inhibitors. Environ Health Perspect 125; doi:10.1289/EHP742.

Bois FY, Maszle D. 1997. MCSim: a simulation program. J Stat Softw 2(9): http://www.jstatsoft.org/v02/i09.

Brown NA, Fabro S. 1981. Quantitation of rat embryonic development in vitro: a morphological scoring system. Teratology 24:65–78; doi:10.1002/tera.1420240108.

Browne H, Mason G, Tang T. 2014. Retinoids and pregnancy: an update. Obstet Gynaecol 16:7–11; doi:10.1111/tog.12075.

Cheng S, Bois FY. 2011. A mechanistic modeling framework for predicting metabolic interactions in complex mixtures. Environ Health Perspect 119:1712–1718; doi:10.1289/ehp.1103510.

Choudhary D, Jansson I, Schenkman JB, Sarfarazi M, Stoilov I. 2003. Comparative expression profiling of 40 mouse cytochrome P450 genes in embryonic and adult tissues. Arch Biochem Biophys 414:91–100; doi:10.1016/S0003-9861(03)00174-7.

Di Renzo, Broccia M, Giavini E, Menegola E. 2007. Citral, an inhibitor of retinoic acid synthesis, attenuates the frequency and severity of branchial arch abnormalities induced by triazole-derivative fluconazole in rat embryos cultured in vitro. Reprod Toxicol 24:326–332; doi:10.1016/j.reprotox.2007.07.012.

Di Renzo, Broccia ML, Giavini E, Menegola E. 2011a. Stage-dependent abnormalities induced by the fungicide triadimefon in the mouse☆. Reprod Toxicol 31:194–199; doi:10.1016/j.reprotox.2010.10.011.

Di Renzo F, Metruccio F, Battistoni M, Moretto A, Menegola E. 2019. Relative potency ranking of azoles altering craniofacial morphogenesis in rats: An in vitro data modelling approach. Food Chem Toxicol 123:553–560; doi:10.1016/j.fct.2018.12.004.

Di Renzo, Rossi F, Prati M, Giavini E, Menegola E. 2011b. Early genetic control of craniofacial development is affected by the in vitro exposure of rat embryos to the fungicide triadimefon. Birth Defects Res B Dev Reprod Toxicol 92:77–81; doi:10.1002/bdrb.20284.

Duester G. 2008. Retinoic acid synthesis and signaling during early organogenesis. Cell 134:921–931; doi:10.1016/j.cell.2008.09.002.

EFSA. 2009. Scientific Opinion on risk assessment for a selected group of pesticides from the triazole group to test possible methodologies to assess cumulative effects from exposure through food from these pesticides to human health.

Feron VJ, Cassee FR, Groten JP. 1998. Toxicology of chemical mixtures: international perspective. Environ Health Perspect 106:1281–1289; doi:10.1289/ehp.98106s61281.

Feron VJ, Groten JP. 2002. Toxicological evaluation of chemical mixtures. Food Chem Toxicol 40:825–839; doi:10.1016/S0278-6915(02)00021-2.

Fujii H. 1997. Metabolic inactivation of retinoic acid by a novel P450 differentially expressed in developing mouse embryos. EMBO J 16:4163–4173; doi:10.1093/emboj/16.14.4163.

Giavini E, Broccia ML, Prati M, Bellomo D, Menegola E. 1992. Effects of ethanol and acetaldehyde on rat embryos developing in vitro. Vitro Cell Dev Biol - Anim 28:205–210; doi:10.1007/BF02631093.

Goldbeter A, Gonze D, Pourquié O. 2007. Sharp developmental thresholds defined through bistability by antagonistic gradients of retinoic acid and FGF signaling. Dev Dyn 236:1495–1508; doi:10.1002/dvdy.21193.

Gordon JE, Shy CM. 1981. Agricultural chemical use and congenital cleft lip and/or palate. Arch Environ Health 36: 213–221.

Groppelli S, Pennati R, De Bernardi F, Menegola E, Giavini E, Sotgia C. 2005. Teratogenic effects of two antifungal triazoles, triadimefon and triadimenol, on Xenopus laevis development: Craniofacial defects. Aquat Toxicol 73:370–381; doi:10.1016/j.aquatox.2005.04.004.

Groten J. 2000. Mixtures and interactions. Food Chem Toxicol 38:S65–S71; doi:10.1016/S0278-6915(99)00135-0.

Hansen JM, Carney EW, Harris C. 1999. Differential alteration by thalidomide of the glutathione content of rat vs. rabbit conceptuses in vitro. Reprod Toxicol 13:547–554; doi:10.1016/S0890-6238(99)00053-2.

Hathcock JN, Hattan DG, Jenkins MY, McDonald JT, Sundaresan PR, Wilkening VL. 1990. Evaluation of vitamin A toxicity. Am J Clin Nutr 52:183–202; doi:10.1093/ajcn/52.2.183.

Hernandez RE, Putzke AP, Myers JP, Margaretha L, Moens CB. 2007. Cyp26 enzymes generate the retinoic acid response pattern necessary for hindbrain development. Development 134:177–187; doi:10.1242/dev.02706.

Hof H. 2001. Critical Annotations to the Use of Azole Antifungals for Plant Protection. Antimicrob Agents Chemother 45:2987–2990; doi:10.1128/AAC.45.11.2987-2990.2001.

Horton C, Maden M. 1995. Endogenous distribution of retinoids during normal development and teratogenesis in the mouse embryo. Dev Dyn 202:312–323; doi:10.1002/aja.1002020310.

Klug S, Lewandowski C, Wildi L, Neubert D. 1989. All-trans retinoic acid and 13-cis-retinoic acid in the rat whole-embryo culture: abnormal development due to the all-trans isomer. Arch Toxicol 63:440–444; doi:10.1007/BF00316445.

Kotch LE, Chen S-Y, Sulik KK. 1995. Ethanol-induced teratogenesis: Free radical damage as a possible mechanism. Teratology 52:128–136; doi:10.1002/tera.1420520304.

Kudoh T, Wilson SW, Dawid IB. 2002. Distinct roles for Fgf, Wnt and retinoic acid in posteriorizing the neural ectoderm. Dev Camb Engl 129: 4335–4346.

Lammer EJ, Chen DT, Hoar RM, Agnish ND, Benke PJ, Braun JT, et al. 1985. Retinoic Acid Embryopathy. N Engl J Med 313:837–841; doi:10.1056/NEJM198510033131401.

Leist M, Ghallab A, Graepel R, Marchan R, Hassan R, Bennekou SH, et al. 2017. Adverse outcome pathways: opportunities, limitations and open questions. Arch Toxicol 91:3477–3505; doi:10.1007/s00204-017-2045-3.

MacLean G, Abu-Abed S, Dollé P, Tahayato A, Chambon P, Petkovich M. 2001. Cloning of a novel retinoic-acid metabolizing cytochrome P450, Cyp26B1, and comparative expression analysis with Cyp26A1 during early murine development. Mech Dev 107:195–201; doi:10.1016/S0925-4773(01)00463-4.

Madden JC, Rogiers V, Vinken M. 2014. Application of in silico and in vitro methods in the development of adverse outcome pathway constructs in wildlife. Philos Trans R Soc B Biol Sci 369:20130584–20130584; doi:10.1098/rstb.2013.0584.

Mark M, Lohnes D, Mendelsohn C, Dupé V, Vonesch JL, Kastner P, et al. 1995. Roles of retinoic acid receptors and of Hox genes in the patterning of the teeth and of the jaw skeleton. Int J Dev Biol 39: 111–121.

Marotta F, Tiboni GM. 2010. Molecular aspects of azoles-induced teratogenesis. Expert Opin Drug Metab Toxicol 6:461–482; doi:10.1517/17425251003592111.

Menegola, Broccia ML, Di Renzo F, Giavini E. 2001. Antifungal triazoles induce malformations in vitro. Reprod Toxicol 15:421–427; doi:10.1016/S0890-6238(01)00143-5.

Menegola, Broccia ML, Di Renzo F, Giavini E. 2003. Pathogenic pathways in fluconazole-induced branchial arch malformations. Birt Defects Res A Clin Mol Teratol 67:116–124; doi:10.1002/bdra.10022.

Menegola, Broccia ML, Di Renzo F, Massa V, Giavini E. 2005a. Craniofacial and axial skeletal defects induced by the fungicide triadimefon in the mouse. Birth Defects Res B Dev Reprod Toxicol 74:185–195; doi:10.1002/bdrb.20035.

Menegola, Broccia ML, Di Renzo F, Massa V, Giavini E. 2004. Relationship between hindbrain segmentation, neural crest cell migration and branchial arch abnormalities in rat embryos exposed to fluconazole and retinoic acid in vitro. Reprod Toxicol 18:121–130; doi:10.1016/j.reprotox.2003.09.004.

Menegola, Broccia ML, Di Renzo F, Massa V, Giavini E. 2005b. Study on the common teratogenic pathway elicited by the fungicides triazole-derivatives. Toxicol In Vitro 19:737–748; doi:10.1016/j.tiv.2005.04.005.

Menegola, Broccia ML, Renzo FD, Prati M, Giavini E. 2000. In vitro teratogenic potential of two antifungal triazoles: triadimefon and triadimenol. Vitro Cell Dev Biol - Anim 36:88; doi:10.1290/1071-2690(2000)036<0088:IVTPOT>2.0.CO;2.

Menegola E, Broccia ML, Di Renzo F, Giavini E. 2006a. Postulated pathogenic pathway in triazole fungicide induced dysmorphogenic effects. Reprod Toxicol 22:186–195; doi:10.1016/j.reprotox.2006.04.008.

Menegola E, Broccia ML, Renzo FD, Giavini E. 2006b. Dysmorphogenic effects of some fungicides derived from the imidazole on rat embryos cultured in vitro. Reprod Toxicol 21:74–82; doi:10.1016/j.reprotox.2005.07.008.

Menegola E, Di Renzo F, Metruccio F, Moretto A, Giavini E. 2013. Effects of mixtures of azole fungicides in postimplantation rat whole-embryo cultures. Arch Toxicol 87:1989–1997; doi:10.1007/s00204-013-1048-y.

Moretto A. 2008. Exposure to multiple chemicals: when and how to assess the risk from pesticide residues in food. Trends Food Sci Technol 19:S56–S63; doi:10.1016/j.tifs.2008.06.004.

Morriss GM, Steele CE. 1977. Comparison of the effects of retinol and retinoic acid on postimplantation rat embryos in vitro. Teratology 15:109–119; doi:10.1002/tera.1420150115.

Morriss GM, Steele CE. 1974. The effect of excess vitamin A on the development of rat embryos in culture. J Embryol Exp Morphol 32: 505–514.

Morriss-Kay G. 1992. Retinoic Acid and Development. Pathobiology 60:264–270; doi:10.1159/000163733.

Mossey PA, Little J, Munger RG, Dixon MJ, Shaw WC. 2009. Cleft lip and palate. The Lancet 374:1773–1785; doi:10.1016/S0140-6736(09)60695-4.

New DAT. 1978. WHOLE-EMBRYO CULTURE AND THE STUDY OF MAMMALIAN EMBRYOS DURING ORGANOGENESIS. Biol Rev 53:81–122; doi:10.1111/j.1469-185X.1978.tb00993.x.

OECD. 2018. Users' Handbook Supplement to the Guidance Document for Developing and Assessing AOPs. Organisation for Economic Co-operation and Development (OECD), Second Edition. Series on Testing and Assessment, No. 233, ENV/JM/MONO(2016)12, OECD Environment, Health and Safety Publications, Paris, France.

Osumi-Yamashita N, Ninomiya Y, Eto K, Doi H. 1994. The contribution of both forebrain and midbrain crest cells to the mesenchyme in the frontonasal mass of mouse embryos. Dev Biol 164:409–419; doi:10.1006/dbio.1994.1211.

Parman T, Wiley MJ, Wells PG. 1999. Free radical-mediated oxidative DNA damage in the mechanism of thalidomide teratogenicity. Nat Med 5:582–585; doi:10.1038/8466.

Pennimpede T, Cameron DA, MacLean GA, Li H, Abu-Abed S, Petkovich M. 2010. The role of CYP26 enzymes in defining appropriate retinoic acid exposure during embryogenesis: CYP26 Enzymes in Mouse Embryonic Development. Birt Defects Res A Clin Mol Teratol 88:883–894; doi:10.1002/bdra.20709.

Piersma AH, Hessel EV, Staal YC. 2017. Retinoic acid in developmental toxicology: Teratogen, morphogen and biomarker. Reprod Toxicol 72:53–61; doi:10.1016/j.reprotox.2017.05.014.

R Development Core Team. 2013. *R: A Language and Environment for Statistical Computing*. R Foundation for Statistical Computing:Vienna, Austria.

Reijntjes S, Blentic A, Gale E, Maden M. 2005. The control of morphogen signalling: Regulation of the synthesis and catabolism of retinoic acid in the developing embryo. Dev Biol 285:224–237; doi:10.1016/j.ydbio.2005.06.019.

Rogers KW, Schier AF. 2011. Morphogen Gradients: From Generation to Interpretation. Annu Rev Cell Dev Biol 27:377–407; doi:10.1146/annurev-cellbio-092910-154148.

Sakai Y. 2001. The retinoic acid-inactivating enzyme CYP26 is essential for establishing an uneven distribution of retinoic acid along the anterio-posterior axis within the mouse embryo. Genes Dev 15:213–225; doi:10.1101/gad.851501.

Schilling TF, Nie Q, Lander AD. 2012. Dynamics and precision in retinoic acid morphogen gradients. Curr Opin Genet Dev 22:562–569; doi:10.1016/j.gde.2012.11.012.

Schneider RA, Hu D, Rubenstein JL, Maden M, Helms JA. 2001. Local retinoid signaling coordinates forebrain and facial morphogenesis by maintaining FGF8 and SHH. Dev Camb Engl 128: 2755–2767.

Sirbu IO. 2005. Shifting boundaries of retinoic acid activity control hindbrain segmental gene expression. Development 132:2611–2622; doi:10.1242/dev.01845.

Steele CE, Marlow R, Turton J, Hicks RM. 1987. In-vitro teratogenicity of retinoids. Br J Exp Pathol 68: 215–223.

Stoilov I, Jansson I, Sarfarazi M, Schenkman JB. 2001. Roles of Cytochrome P450 in Development. Drug Metabol Drug Interact 18; doi:10.1515/DMDI.2001.18.1.33.

Suzuki T, Oohara I, Kurokawa T. 1999. Retinoic acid given at late embryonic stage depresses sonic hedgehog and Hoxd-4 expression in the pharyngeal area and induces skeletal malformation in flounder

(Paralichthys olivaceus) embryos. Dev Growth Differ 41:143–152; doi:10.1046/j.1440-169x.1999.00420.x.

Tahayato A, Dollé P, Petkovich M. 2003. Cyp26C1 encodes a novel retinoic acid-metabolizing enzyme expressed in the hindbrain, inner ear, first branchial arch and tooth buds during murine development. Gene Expr Patterns 3:449–454; doi:10.1016/S1567-133X(03)00066-8.

Tiboni GM, Marotta F, Carletti E. 2009. Fluconazole alters CYP26 gene expression in mouse embryos. Reprod Toxicol 27:199–202; doi:10.1016/j.reprotox.2009.01.001.

Trainor PA, Krumlauf R. 2000. Patterning the cranial neural crest: hindbrain segmentation and Hox gene plasticity. Nat Rev Neurosci 1:116–124; doi:10.1038/35039056.

Uehara M, Yashiro K, Mamiya S, Nishino J, Chambon P, Dolle P, et al. 2007. CYP26A1 and CYP26C1 cooperatively regulate anterior–posterior patterning of the developing brain and the production of migratory cranial neural crest cells in the mouse. Dev Biol 302:399–411; doi:10.1016/j.ydbio.2006.09.045.

Villeneuve DL, Crump D, Garcia-Reyero N, Hecker M, Hutchinson TH, LaLone CA, et al. 2014. Adverse Outcome Pathway (AOP) Development I: Strategies and Principles. Toxicol Sci 142:312–320; doi:10.1093/toxsci/kfu199.

Warkany J, Schraffenberger E. 1944. Congenital Malformations of the Eyes Induced in Rats by Maternal Vitamin A Deficiency. Exp Biol Med 57:49–52; doi:10.3181/00379727-57-14695P.

White RJ, Nie Q, Lander AD, Schilling TF. 2007. Complex regulation of cyp26a1 creates a robust retinoic acid gradient in the zebrafish embryo. PLoS Biol 5:e304; doi:10.1371/journal.pbio.0050304.

White RJ, Schilling TF. 2008. How degrading: CYP26S in hindbrain development. Dev Dyn 237:2775–2790; doi:10.1002/dvdy.21695.

Whiting J. 1997. Craniofacial abnormalities induced by the ectopic expression of homeobox genes. Mutat Res Mol Mech Mutagen 396:97–112; doi:10.1016/S0027-5107(97)00177-2.

Zarn JA, Brüschweiler BJ, Schlatter JR. 2002. Azole Fungicides Affect Mammalian Steroidogenesis by Inhibiting Sterol 14α-Demethylase and Aromatase. Environ Health Perspect 111:255–261; doi:10.1289/ehp.5785.

Zgheib E, Gao W, Limonciel A, Aladjov H, Yang H, Tebby C, et al. submitted. Application of three approaches for quantitative AOP development to renal toxicity. Comput Toxicol.

9 Tables

Table 1: Counts of branchial arch malformations observed in embryos exposed to retinoic acid, flusilazole, triadimefon, cyproconazole and binary mixtures of the last three molecules.

Treatment	Dose (µM)	Malformed embryos	Observed embryos
Retinoic Acid (RA)	0	0	22
	0.025	2	23
	0.05	11	16
	0.125	19	19
	0.25	15	17
	0.5	28	28
Flusilazole (FLUSI)	0	0	18
	1.5625	0	10
	3.125	5	11
	6.25	9	9
	9.375	5	5
Triadimefon (FON)	0	0	9
	6.25	0	8
	7.8	5	12
	12.5	3	11
	15	6	10
	25	8	8
	31.5	6	7
	50	7	7
	250	4	4
Cyproconazole (CYPRO)	0	0	9
	7.8	4	14
	15	8	9
	31.5	7	7
	250	3	3
FLUSI (+ FON 12.5 µM)	0	0	22
	1.5625	4	7
	3.125	11	12
	6.25	6	6
	9.375	6	6
FON (+ FLUSI 3.125 µM)	0	0	22
	6.25	10	10
	12.5	11	12
	25	8	8
	50	7	7
CYPRO (+ FON 7.8 µM)	0	0	9
	7.8	9	11
	15	3	3

Table 2: Model parameter values for retinoic acid gradient perturbation model.

Parameter	Symbol	Value (units)	Reference
RA synthesis rate constant	$k_{syn,RA}$	0.59 (nM/s)	(Horton and Maden 1995)
RA metabolic rate constant	$k_{met,RA}$	0.0167 (1/nM/s)	(Goldbeter et al. 2007)
RA degradation rate constant	$k_{deg,RA}$	0 (1/s)	(Goldbeter et al. 2007)
Amount of ADH	*ADH*	7.1 (nM)	(Goldbeter et al. 2007)
cyp26a1 base transcription rate	k_{trs}	0.0061 (nM/s)	(Goldbeter et al. 2007)
Maximum increase in transcription	v_{max}	0.118 (nM/s)	(Goldbeter et al. 2007)
Transcription activation by RA constant	k_{act}	7.08 (nM)	- [a]
Transcription inhibition by FGF constant	k_{inh}	1 (nM)	- [a]
CYP26 mRNA degradation rate constant	$k_{deg,mRNA}$	0.0167 (1/s)	(Goldbeter et al. 2007)
CYP26 translation rate constant	k_{tsl}	0.0167 (1/s)	(Goldbeter et al. 2007)
CYP26 degradation rate constant	$k_{deg,CYP26}$	0.00467 (1/s)	(Goldbeter et al. 2007)
FGF synthesis rate	$k_{syn,FGF}$	0.083 (mM/s)	(Goldbeter et al. 2007)
FGF degradation rate constant	$k_{deg,FGF}$	0.0167 (1/s)	(Goldbeter et al. 2007)
CYP26 inhibition by CYP26 constant	$k_{inh,FLUSI}$	- (1/μM/s)	- [b]
CYP26 inhibition by FON constant	$k_{inh,FON}$	- (1/μM/s)	- [b]
CYP26 inhibition by CYPRO constant	$k_{inh,CYPRO}$	- (1/μM/s)	- [b]

[a] These parameters were adjusted to give match information about RA, and CYP gradients.

[b] These parameters were statistically calibrated with data.

Table 3: Model parameter values for retinoic acid gradient perturbation model.

Parameter	Unit	Mode	Mean	SD	95% CI
$k_{inh,FLUSI}$	1/μM/s	0.0033	0.0035	0.00088	0.0020 – 0.0055
$k_{inh,FON}$	1/μM/s	0.00077	0.00080	0.00015	0.00054 – 0.0011
$k_{inh,CYPRO}$	1/μM/s	0.0012	0.0013	0.00033	0.00073 – 0.0020
Q_0	-	2×10^{-7}	0.0050	0.0051	0.00015 – 0.019
Q_1	1/nM	0.014	0.015	0.0025	0.010 – 0.020

[a] These parameters were adjusted to give match information about RA, and CYP gradients.

[b] These parameters were statistically calibrated with data.

10 Figure legends

Figure 1: AOP structure for branchial arch malformations during embryogenesis (between days 9.5 and 10 post-fertilization, in the rat). There is a feedback between the molecular initiating event (MIE) and the first key event (KE).

Figure 2: Simulated gradient profiles for RA, CYP26A1 mRNA, CYP26A1 and FGF in the rat embryo at day 10 post-fertilization, for various levels of exposure to FLUSI.

Figure 3: Fitted relationship between branchial arch malformations and retinoic acid concentration increase above background. The black line corresponds to the best fit of the multistage model, the dark grey area marks the 95% confidence region of the malformation probability estimates, the light grey area the 95% confidence regions of model predictions for groups of 12 embryos, the red dots are the data values (with 95% binomial confidence limits).

Figure 4: Estimated relationship between branchial arch malformations and concentrations of three CYP26A1 inhibitors. The black lines correspond to the best fit of the multistage model, the dark grey areas mark the 95% confidence region of the malformation probability estimates, the light grey areas the 95% confidence regions of model predictions for groups of 12 embryos, the red dots are the data values (with 95% binomial confidence limits).

Figure 5: Fitted relationship between mid-hindbrain retinoic acid concentrations and constant exposure levels to three CYP26A1 inhibitors. The red lines correspond to the best prediction by the RA gradient formation model, the grey areas mark the 95% confidence region of the model predictions.

Figure 6: Predicted relationship between branchial arch malformations and concentrations of mixtures of three CYP26A1 inhibitors. No data fitting was made. The black lines correspond to the best fit of the multistage model, the dark grey areas mark the 95% confidence region of the malformation probability estimates, the light grey areas the 95% confidence regions of model predictions for groups of 12 embryos, the red dots are the data values (with 95% binomial confidence limits).

Figure 7: Model of shifting RA boundaries during mouse hindbrain segmentation adapted from Sirbu et al., 2005. Initially, RA forms an early anterior boundary at r2/r3 (next to the r2 border of Cyp26a1

expression), followed soon after by a late anterior boundary at r4/r5 (next to the r4 border of Cyp26c1 expression). At E8.5, Cyp26b1 is expressed in r3 and r5 while Cyp26c1 is expressed in r2 and r4.

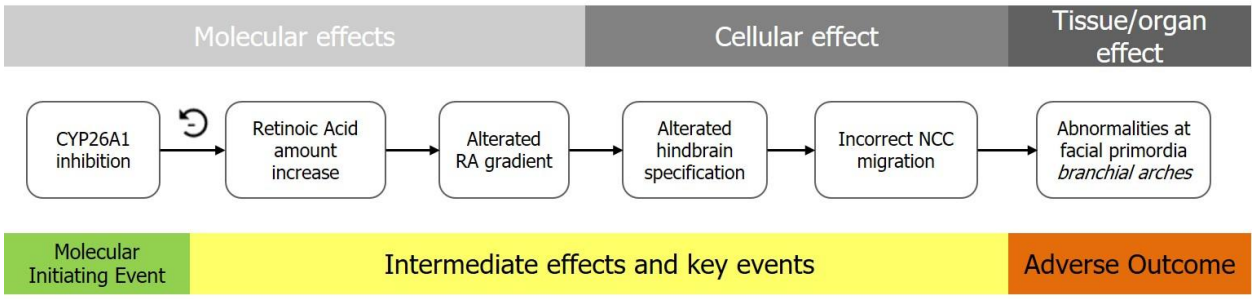

Figure 1: AOP structure for branchial arch malformations during embryogenesis (between days 9.5 and 10 post-fertilization, in the rat). There is a feedback between the molecular initiating event (MIE) and the first key event (KE).

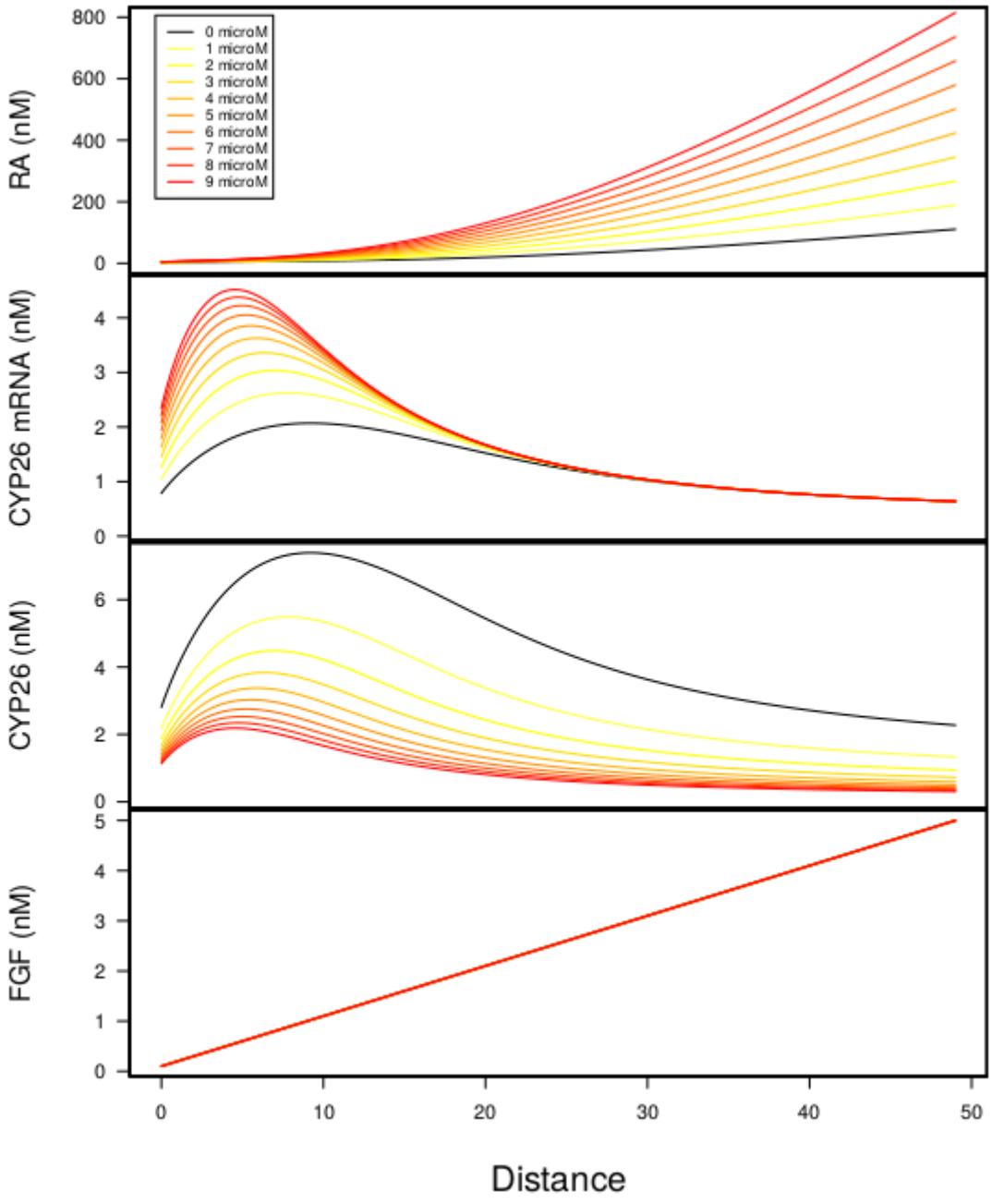

Figure 2: Simulated gradient profiles for RA, CYP26A1 mRNA, CYP26A1 and FGF in the rat embryo at day 10 post-fertilization, for various levels of exposure to FLUSI.

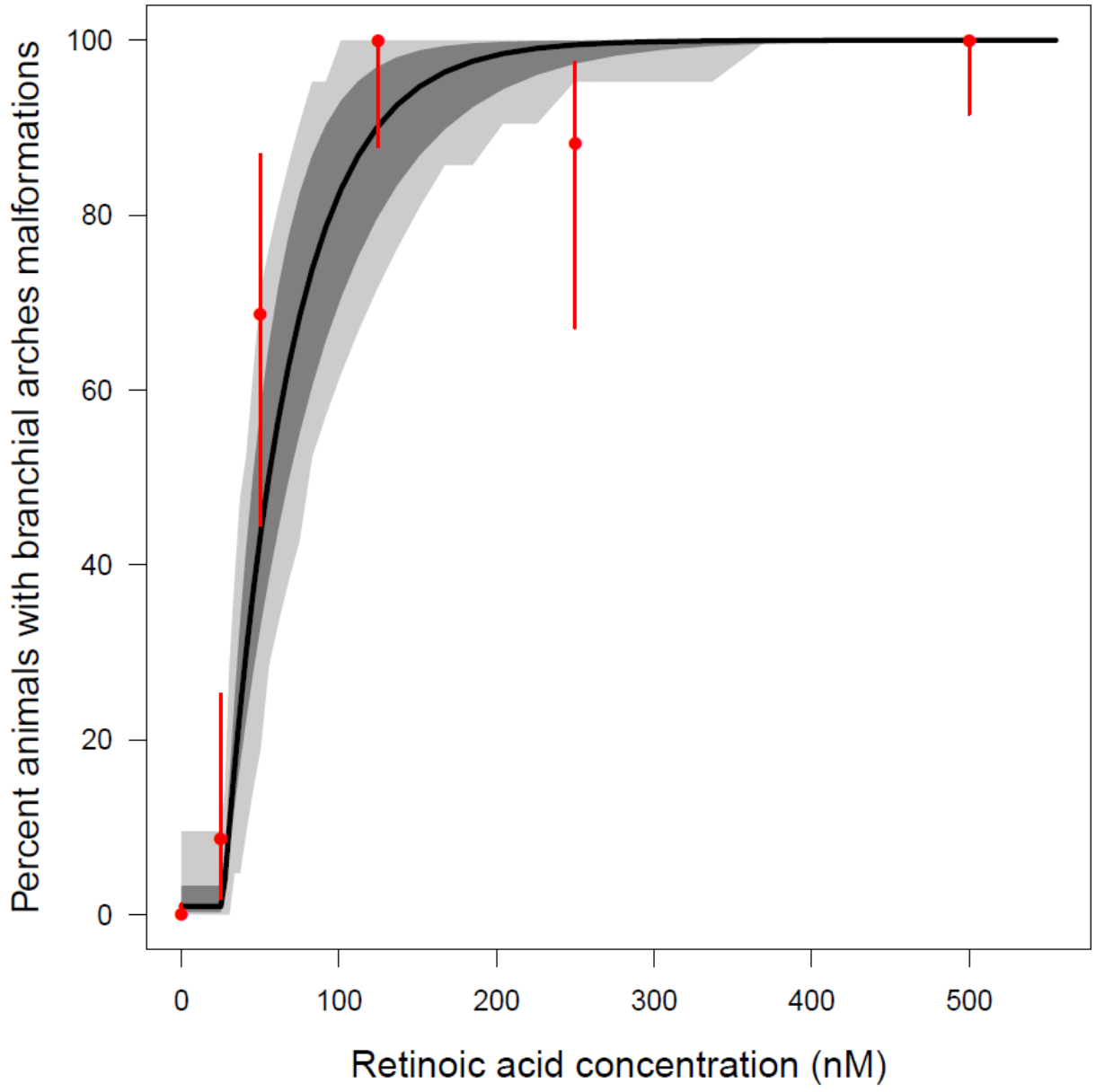

Figure 3: Fitted relationship between branchial arch malformations and retinoic acid concentration increase above background. The black line corresponds to the best fit of the multistage model, the dark grey area marks the 95% confidence region of the malformation probability estimates, the light grey area the 95% confidence regions of model predictions for groups of 12 embryos, the red dots are the data values (with 95% binomial confidence limits).

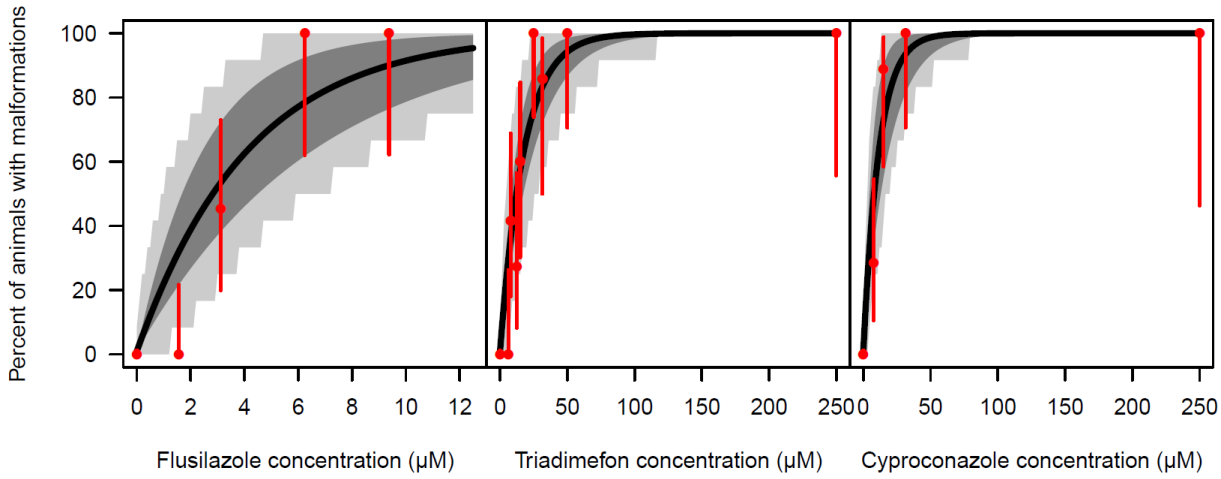

Figure 4: Fitted relationship between branchial arch malformations and concentrations of three CYP26A1 inhibitors. The black lines correspond to the best fit of the multistage model, the dark grey areas mark the 95% confidence region of the malformation probability estimates, the light grey areas the 95% confidence regions of model predictions for groups of 12 embryos, the red dots are the data values (with 95% binomial confidence limits).

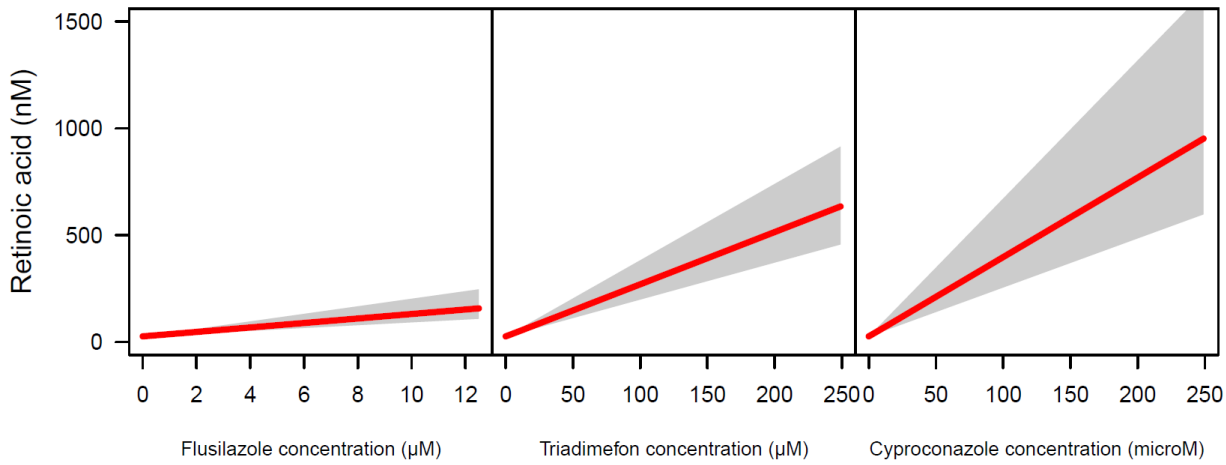

Figure 5: Estimated relationship between mid-hindbrain retinoic acid concentrations and constant exposure levels to three CYP26A1 inhibitors. The red lines correspond to the best prediction by the RA gradient formation model, the grey areas mark the 95% confidence region of the model predictions.

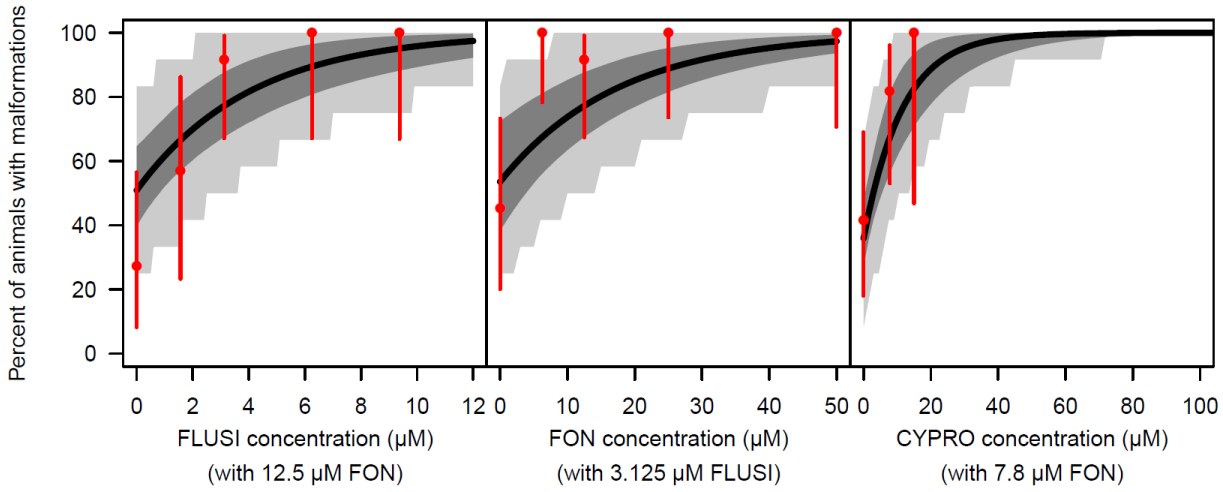

Figure 6: Predicted relationship between branchial arch malformations and concentrations of mixtures of three CYP26A1 inhibitors. No data fitting was made. The black lines correspond to the best fit of the multistage model, the dark grey areas mark the 95% confidence region of the malformation probability estimates, the light grey areas the 95% confidence regions of model predictions for groups of 12 embryos, the red dots are the data values (with 95% binomial confidence limits).

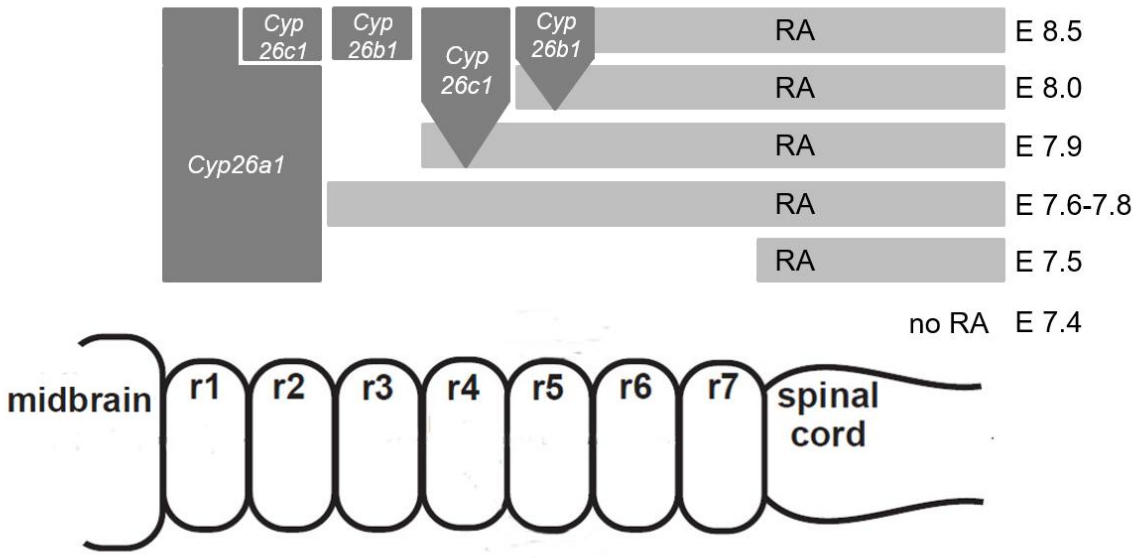

Figure 7: Model of shifting RA boundaries during mouse hindbrain segmentation adapted from Sirbu et al., 2005. Initially, RA forms an early anterior boundary at r2/r3 (next to the r2 border of Cyp26a1 expression), followed soon after by a late anterior boundary at r4/r5 (next to the r4 border of Cyp26c1 expression). At E8.5, Cyp26b1 is expressed in r3 and r5 while Cyp26c1 is expressed in r2 and r4.

Highlights

- Development of a quantitative AOP for craniofacial malformations in rat embryos
- Perturbation of retinoic acid pathway after exposure to azole fungicide mixtures
- Possible mechanistic and predictive applications in pesticides risk assessment